

Effect vapor grown carbon nanofiber on thermal and mechanical properties of epoxy

Yuanxin Zhou · Farhana Pervin · Shaik Jeelani

Received: 12 September 2006 / Accepted: 15 February 2007 / Published online: 30 May 2007
© Springer Science+Business Media, LLC 2007

Abstract In the present investigation, dynamic mechanical analysis (DMA), thermo gravimetric analysis (TGA), tensile tests, fatigue tests and the single edge notch tensile (SENT) tests were performed on unfilled, 1, 2 and 3 wt.% vapor grown carbon nanofiber (CNF) filled SC-15 epoxy to identify the loading effect on thermal and mechanical properties of the composites. DMA studies revealed that filling the 3% carbon nanofiber into epoxy can produce 65% enhancement in storage modulus at room temperature and 6 °C increase in T_g . However, TGA results show that thermal stability of composite is insensitive to the CNF content. Tensile tests were carried out at the strain rate range from 0.02 min⁻¹ to 2 min⁻¹. Results show that CNF/epoxy are strain rate sensitive materials, the modulus and tensile strength increased with increasing of strain rate. Experimental results also indicate that modulus of the nanophased epoxy increases continuously with increasing CNF content. But the 2% CNF infusion system exhibit maximum enhancement in tensile strength, fatigue performance and fracture toughness as compared with other system.

Introduction

Epoxy resin has been of significant importance to the engineering community for many years. Components made of epoxy based materials have provided outstand-

ing mechanical, thermal, and electrical properties [1]. Using an additional phase (e.g., inorganic fillers) to strengthen the properties of epoxy resins has become a common practice [2]. The use of these fillers has been proven to improve the material properties of epoxy resins. Based on the fact that micro scale fillers have successfully been synthesized with epoxy resin [3–6], nano-scaled materials are now being considered as filler material to produce high performance composite structures with further enhanced properties. Improvements in mechanical, electrical, and chemical properties have resulted in major interests in nanocomposite materials in numerous automotive, aerospace, electronics and biotechnology applications [7–8].

Vapor grown carbon nanofibers (CNFs) due to their high tensile strength, modulus and relatively low cost are drawing significant attention for its potential applications in nano-scale polymer reinforcement. It is synthesized from pyrolysis of hydrocarbons or carbon monoxide in the gaseous state, in the presence of a catalyst [9–10]. Vapor grown CNFs distinguish themselves from other types of nanofibers, such as polyacrylonitrile or mesophase pitch-based carbon fiber, in its method of production, physical properties and structure. Thermoplastic such as polypropylene [11–16], polycarbonate [17–21], nylon [22], thermosets such as epoxy [23] as well as thermoplastic elastomers such as butadiene-styrene diblock copolymer [24] have been reinforced with carbon nanofibers.

The primary interest of this paper was to characterize the effect of vapor grown CNF addition on the thermal and mechanical behavior of epoxy. DMA, TGA, tensile, fracture and fatigue tests will be performed on unfilled, 1, 2 and 3 wt.% CNF filled SC-15 epoxy to identify the optimal the loading of CNF.

Y. Zhou (✉) · F. Pervin · S. Jeelani
Tuskegee University's Center for Advanced Materials (T-CAM),
100 Chappie James Center, Tuskegee, AL 36088, USA
e-mail: yzhou@tuskegee.edu

Experimental

The resin used in this study is a commercially available SC-15 epoxy obtained from *Applied Poleramic, Inc.* It is a low viscosity two phased toughened epoxy resin system consisting of part-A (resin mixture of Diglycidylether of Bisphenol-A, Aliphatic Diglycidylether epoxy toughner) and part-B (hardener mixture of, cycloaliphatic amine and polyoxylalkylamine). The carbon nano fibers are obtained from Applied Science Inc (154 W Xenia Ave. Cedarville, OH). The fiber diameters is in the 200 nm and the fiber length is range from 20 μm to 100 μm . The weight fraction of carbon nano fibers are range from 0 wt.% to 3 wt.% (corresponding to CNF volume fraction of 0, 0.63, 1.27 and 1.90%) to identify an optimal loading giving the best thermal and mechanical properties.

Pre-calculated amount of carbon nanofiber and part-A were mixed together in a suitable beaker. The mixing was carried out through a high intensity ultrasonic irradiation (Ti-horn, 20 kHz *Sonics Vibra Cell, Sonics Mandmaterials, Inc, USA*) for half an hour with pulse mode (50 s on/25 s off). To avoid a temperature rise during the sonication process, external cooling was employed by submerging the beaker containing the mixture in an ice-bath. Once the irradiation was completed, part-B was added to the modified part-A then mixed using a high speed mechanical stirrer for about 10 min. The mix-ratio of part A and part B of SC-15 is 10:3. The rigorous mixing of part-A and part-B produced highly reactive volatile vapor bubbles at initial stages of the reaction, which could detrimentally affect the properties of the final product by creating voids. A high vacuum was accordingly applied using *Brand Tech Vacuum* system for about 30 min. After the bubbles were completely removed, the mixture was transferred into a plastic and Teflon coated metal molds and kept for 24 h at room temperature. The cured material was then de-molded and trimmed. Finally, test samples were machined for thermal and mechanical characterization. All as-prepared panels were post-cured at 100 °C for 5 h, in a Lindberg/Blue Mechanical Convection Oven.

Dynamic Mechanic analysis (DMA) was performed on a TA Instruments 2,980 operating in the three-point bending mode at an oscillation frequency of 1 Hz. Data were collected from room temperature to 160 °C at a scanning rate of 10 °C/min. The sample specimens were cut by a diamond saw in the form of rectangular bars of a nominal 4 mm \times 30 mm \times 12 mm. Thermo gravimetric Analysis (TGA) was conducted with a TA Instruments TGA2950 at a heat rate of 10 °C/min from ambient to 600 °C. The TGA samples were cut into small pieces using ISOMET Cutter and were machined using the mechanical grinder to maintain the sample weight of about 5–20 mg range. The real time characteristic curves were generated by *Universal*

Analysis 2000-TA Instruments Inc., data acquisition system.

Uniaxial tensile tests were performed on an MTS hydraulic testing machine. The machine was run under displacement control mode at a crosshead speed of 10, 1 and 0.1 mm/min. Since the gage length was 50 mm, the average strain rates were assumed to be 2, 0.2 and 0.02 min^{-1} . Three parameters were determined from each stress–strain curve: elastic modulus (E) from the initial slope of the stress–strain curve, tensile strength (σ_b) corresponding to the maximum stress, and failure strain (ϵ_b).

Stress-controlled tension–tension fatigue tests were performed at 21.5 °C. The ratio of the minimum cyclic stress and the maximum cyclic stress, i.e., the *R*-ratio, was 0.1. A cyclic frequency of 1 Hz was used to reduce the possibility of thermal failure. The stress concentration effect was study on 2 wt.% CNF/Epoxy by introducing central holes in the specimens. The diameters of the hole are 1/4 width and 1/8 width. The theoretical stress concentration factors are 2.43 and 2.64.

The single edge notch tensile (SENT) specimens were cast in a metal mold without the notch. The specimens were pre-cracked 8 mm by the diamond saw and crack was extended to 2 mm by tapping a fresh razor blade, frozen in the liquid nitrogen, into the notch. The specimen size is 120 mm in length, 20 mm in width and 3.5 mm in thickness. At least four samples for each material were used.

The critical stress intensity factor, K_{Ic} was calculated according to the following equation:

$$K_{Ic} = \frac{P}{B\sqrt{W}}f(a/w) \quad (1)$$

where, P = applied load on the specimen; B = specimen thickness; W = specimen width; a = crack length and

$$f(a/w) = \frac{\sqrt{2 \tan \frac{\pi a}{2w}}}{\cos \frac{\pi a}{2w}} \left[0.752 + 2.02 \left(\frac{a}{w} \right) + 0.37 \left(1 - \sin \frac{\pi a}{2w} \right)^3 \right]$$

Results and discussions

Thermal properties

Figure 1 illustrates the DMA plots of storage modulus versus temperature as a function of carbon nanofiber loading. It can be seen that the storage modulus steadily increased with an increasing fiber weight percent. The addition of 3 wt.% of carbon nanofiber yielded a 65% increase of the storage modulus at 30 °C. The loss factor, $\tan \delta$, curve of the neat epoxy and its CNF/epoxy nanocomposites measured by DMA are shown in Fig. 2. The

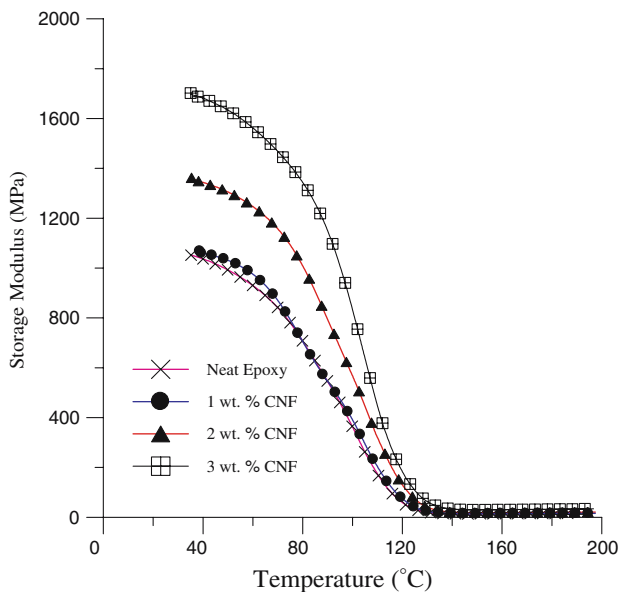


Fig. 1 Storage modulus vs. temperature of CNFs modified epoxy

peak height of loss factor decreased with increasing carbon nanofiber content, but the T_g , determined from the peak position of $\tan\delta$, increased with increasing fiber content. There was a broadening of the peak due to the unconstrained segments of the polymer molecules retained the T_g . But those segments close to the nanofiller surface were less mobile, which led to an increase in T_g (Fig. 3).

The peak factor, Γ , is defined as the full width at half maximum of the $\tan\delta$ peak divided by its height, and it can

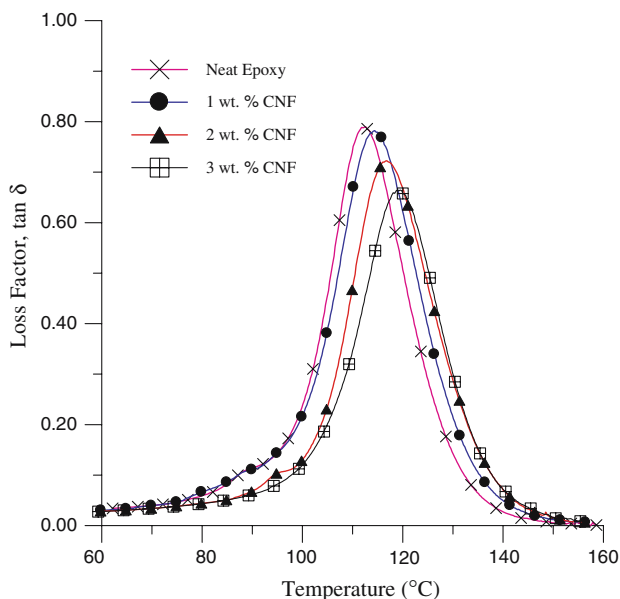


Fig. 2 Loss factor vs. temperature of CNFs modified epoxy

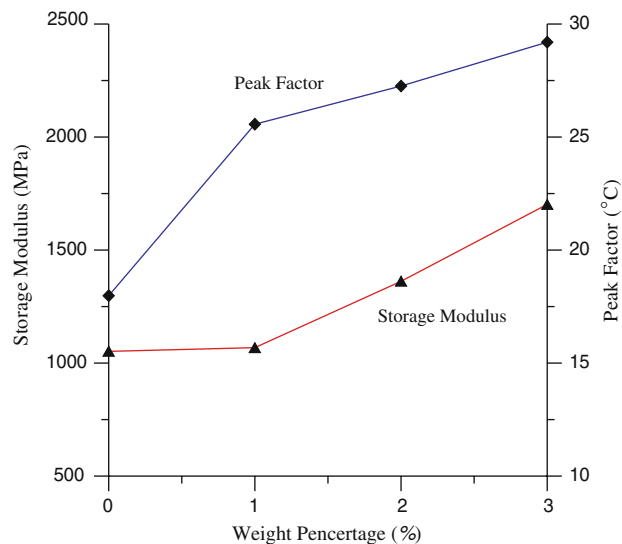


Fig. 3 Effect of CNF content on storage modulus and peak factor of epoxy

be qualitatively used to assess the homogeneity of epoxy network. The neat epoxy was observed to have a low peak factor that indicated the crosslink density and homogeneity of the epoxy network were high. For the nanophased epoxy, the peak factor increased with increasing CNF weight percent, as shown in Fig. 4, and it exhibited a broadened $\tan\delta$ peak on the high temperature side of the DMA profile. The higher peak factor for the nanophased epoxy is indicative of lower crosslink density and greater heterogeneity, which suggests intercalation of CNF into the epoxy network.

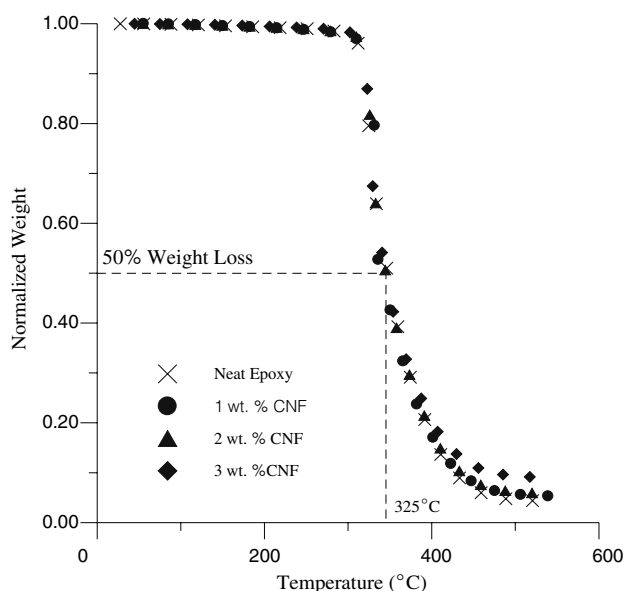


Fig. 4 Loss weight vs. temperature of CNFs modified epoxy

Figure 4 shows the TGA of all categories of nanocomposites considered for this investigation. We define the 50% weight loss as a marker for structural decomposition of the samples. In this figure, the decomposition temperatures are almost the same, indicating the CNF content had no effect on the decomposition temperature of epoxy.

Tensile response

Tensile stress–strain curves of neat epoxy and nanophased epoxy at different strain rate are shown in Fig. 5a–d. All specimens failed immediately after the tensile stress reached the maximum value; however, the stress–strain curves showed considerable non-linearity before reaching the maximum stress, but no obvious yield point was found in the curves. Five specimens were tested for each condition. The average properties obtained from these tests are listed in Table 1. Figure 5 also show the effect of strain rate on the stress–strain curves of neat and nanophased epoxy. Both the modulus and tensile strength increase with increasing strain rate, but the failure strain decreases with increasing strain rate.

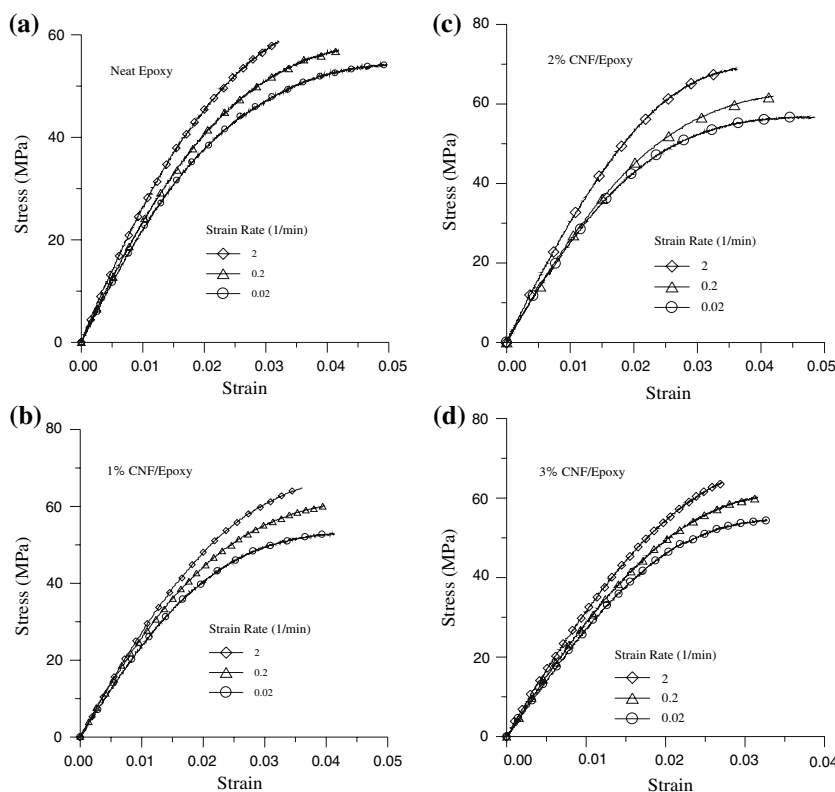
Figure 6 shows comparison of stress–strain curves of the composite at the same strain rate (2 min⁻¹). The modulus of the nanophased epoxy increases continuously with increasing CNF content. An improvement of about 19.4%

Table 1 Tensile properties of neat and nanophased epoxy

CNF contents	Strain rate (1/min)	Tensile modulus (GPa)	Tensile strength (MPa)	Failure strain (%)
Neat	0.02	2.31 ± 0.12	53.01 ± 2.79	4.86 ± 0.34
	0.2	2.49 ± 0.17	57.04 ± 2.32	4.18 ± 0.29
	2	2.78 ± 0.16	58.78 ± 2.65	3.20 ± 0.17
1% CNF/Epoxy	0.02	2.39 ± 0.20	54.30 ± 2.45	4.06 ± 0.21
	0.2	2.64 ± 0.11	60.14 ± 2.73	3.77 ± 0.21
	2	2.87 ± 0.21	64.84 ± 2.27	3.61 ± 0.23
2% CNF/Epoxy	0.02	2.63 ± 0.14	56.75 ± 3.13	4.68 ± 0.33
	0.2	2.89 ± 0.17	62.49 ± 2.43	4.01 ± 0.29
	2	3.17 ± 0.15	68.98 ± 2.35	3.60 ± 0.23
3% CNF/Epoxy	0.02	2.84 ± 0.22	53.82 ± 3.06	3.36 ± 0.27
	0.2	3.03 ± 0.19	60.24 ± 2.48	3.18 ± 0.17
	2	3.44 ± 0.21	63.96 ± 3.03	2.75 ± 0.20

in tensile modulus was observed with an addition of 3 wt.% of CNF. However, Table 1 and Fig. 6 also show that the system with 2 wt.% infusion is the best system with 17.4% enhancement in tensile strength. The strength begins to degrade with 3 wt.% loading, although the gain in modulus is maintained. The relationship between modulus, strength, and CNF weight fraction was plotted in Fig. 7.

Fig. 5 Stress strain curves of neat and nanophased epoxy at different strain rate (a: Neat epoxy; b: 1%CNF/epoxy; c: 2%CNF/epoxy and d: 3%CNF/epoxy)



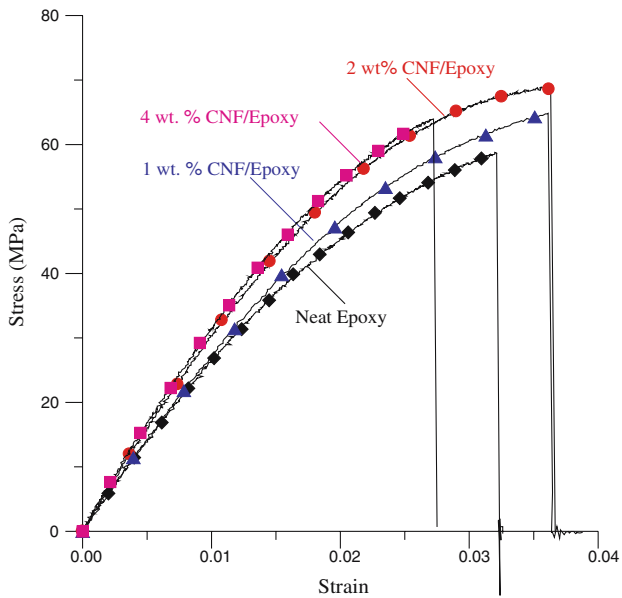


Fig. 6 Effect of CNF weight fraction on stress strain curves of epoxy (strain rate is 2 min^{-1})

Strain rate sensitivity of tensile strength

From Fig. 5 and Table 1, it can be concluded that neat and nanophased epoxy are strain rate sensitive materials. Figure 8a and b show the variation of modulus E and tensile strength σ_b with $\ln \dot{\epsilon}$ for four kinds of materials. The relationships between E and $\ln \dot{\epsilon}$ as well as σ_Y and $\ln \dot{\epsilon}$ can be represented by single straight lines, the slopes of which give information about the strain rate sensitivities of modulus and yield strength, respectively. The following

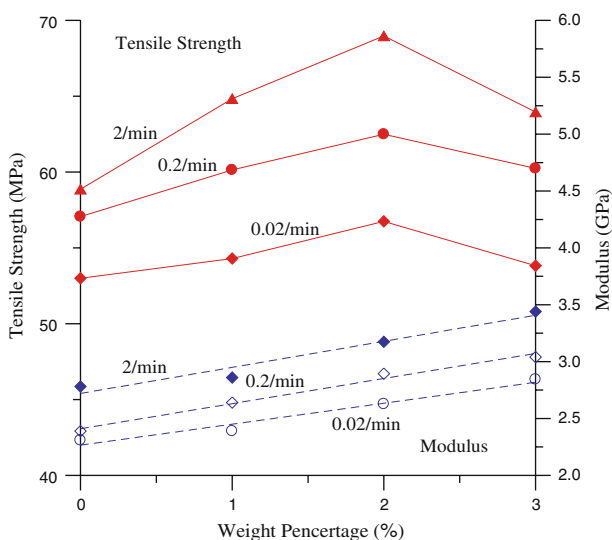


Fig. 7 Effect of CNF content on tensile modulus and tensile strength of epoxy

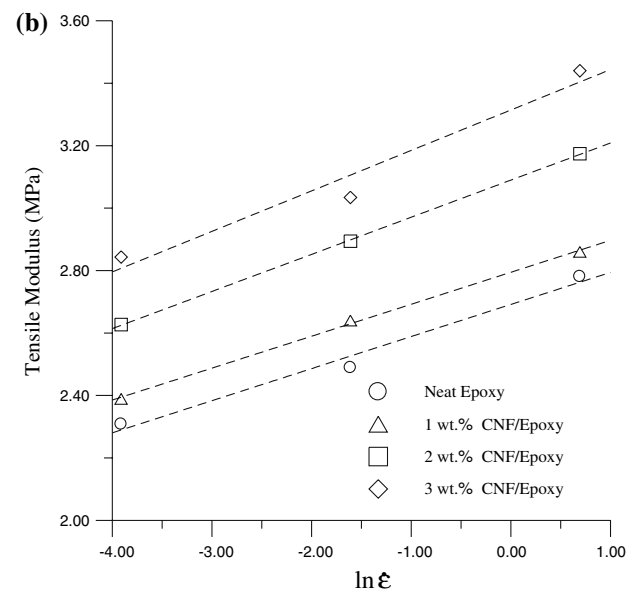
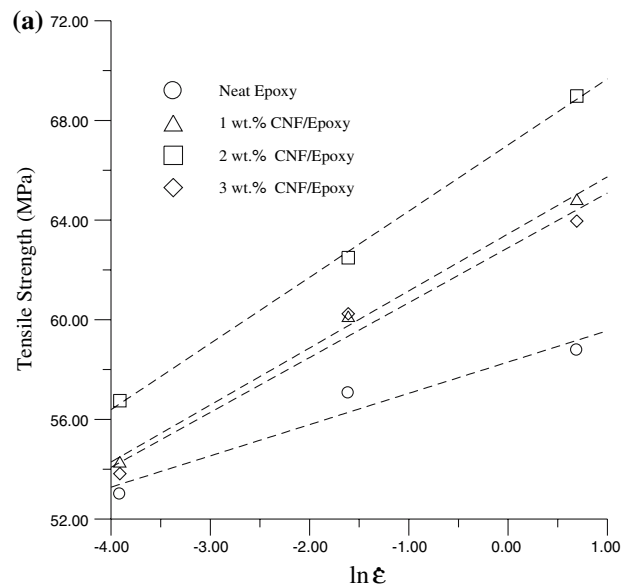


Fig. 8 Effect of strain rate on the tensile strength (a) and the tensile modulus (b) of neat and nanophased epoxy

relationships were found to fit the relationship between modulus, yield strength and strain rate of these three materials.

$$E = E_0 \left(1 + \lambda_1 \ln \frac{\dot{\epsilon}}{\dot{\epsilon}_0} \right) \quad (2a)$$

$$\sigma_Y = \sigma_{Y0} \left(1 + \lambda_2 \ln \frac{\dot{\epsilon}}{\dot{\epsilon}_0} \right) \quad (2b)$$

where, E_0 , σ_{Y0} and $\dot{\epsilon}_0$ are reference elastic modulus, reference yield strength and reference strain rate, respectively. Two other parameters, $\lambda_{1,2}$ appearing in

Table 2 Constitutive parameters of neat nanophased epoxy

Materials	λ_1	λ_2	V (nm) ³	σ_f (MPa)	b
Neat	0.130	1.26	3.23	55.5	-0.0471
1% CNF/Epoxy	0.119	2.29	1.78	68.3	-0.0676
2% CNF/Epoxy	0.102	2.66	1.53	115.6	-0.0981
3% CNF/Epoxy	0.102	2.20	1.85	103.6	-0.104

Eqs. (2a) and (2b) are defined as strain rate strengthening coefficient. Mathematically, they are defined as

$$\lambda_{1,2} = \frac{\partial(E, \sigma_y)}{\partial \ln \dot{\epsilon}} \tag{3}$$

The values of strain rate strength coefficient are calculated from the experimental results using the least square method and are given in Table 2. It can be observed that strain rate strengthening coefficient increase as the CNF content is increased up to 2%; however, at 3%, strain rate strengthening coefficient is decreased. The dashed lines in Fig. 8 are simulated results, which fit the experimental data well. According to the Eyring equation, the activation volume of the material can be obtain from the strain rate strengthening coefficient as follows

$$V = \frac{RT}{\lambda_2} \tag{4}$$

where, V is activation volume, R is Gas constant, and T is the temperature. The activation volume of the neat and nanophased epoxy were calculated using the tensile strength data in Table 1. It was observed in Table 2 that filling CNF can reduce the activation volumes, and a maximum 53% reduction in the activation volumes was found in 2% system as compared with neat system. The higher tensile strength and lower activation volumes of nanocomposite are attributed to the restricted segmental motions in the neighborhood of CNF/Epoxy interfaces.

Fatigue performance

Figure 9 shows the fatigue $S-N$ curves of the neat and nanophased epoxy at ambient temperature. In this figure, the vertical axis or the S -axis represents the maximum cyclic stress and the horizontal axis or the N -axis represents the number of cycles to failure. At the same stress level, the fatigue life of nanophased epoxy was significantly higher than that of the neat epoxy. Based on the experimental data, following equations were established for the $S-N$ curves of for materials:

$$\sigma = \sigma_f(Nf)^b \tag{5}$$

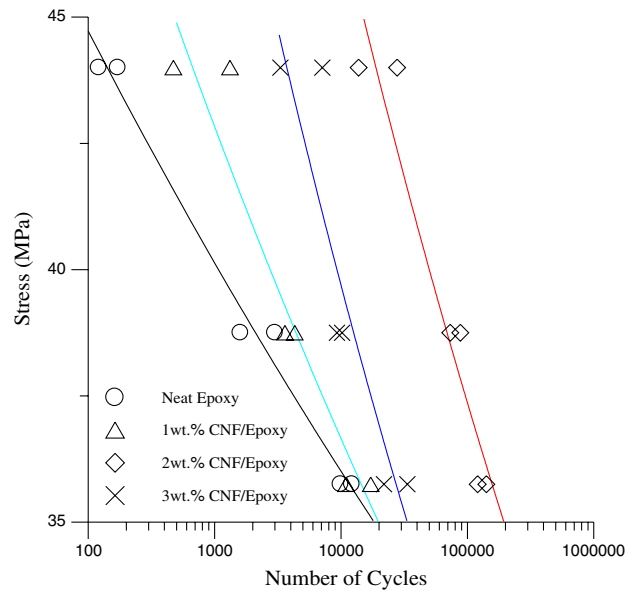


Fig. 9 $S-N$ curves of epoxy and nanocomposite

The values of fatigue strength coefficient σ_f and fatigue strength exponent b with different CNF contents are listed in the Table 2. In this table, fatigue strength exponent decrease with increasing weight fraction of CNF, while the fatigue strength coefficient increases as the CNF content is increased up to 2%; however, at 3%, the fatigue strength coefficient is decreased. Figure 10 shows the fatigue life vs. CNF weight fraction at different cycling stress levels. 2 wt.% CNF/Epoxy exhibit the highest fatigue performance.

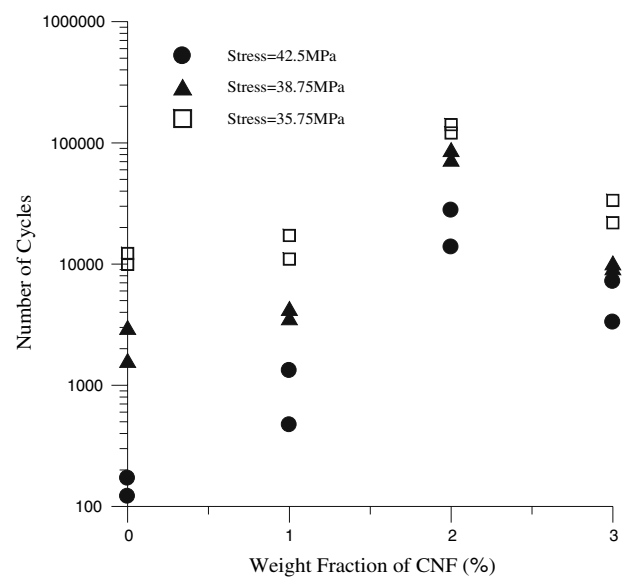


Fig. 10 Effect of CNF contents on fatigue life of epoxy

Figure 11a shows the $S-N$ curves of 2 wt.% CNF/Epoxy specimens containing a central hole. For comparison, the $S-N$ curve for the unnotched specimen is also shown. In this figure, the stress for the notched specimens was calculated based on the gross area of the specimen. The fatigue strength was lower for specimens containing a central hole. Additionally, the fatigue strength decreased with increasing hole diameter. However, when the stress was calculated based on the net area, the fatigue strengths of samples with central

hole were overlap, which are lower than that of samples without hole (as shown in Fig. 11b). The theoretical stress concentration factor for specimens with holes of diameters of 1.6 mm and 3.2 mm are 2.66 and 2.43. This indicates that CNF/Epoxy nanocomposite has notch sensitivity, but the different stress concentration factor has the same effect on the fatigue life of composite. To investigate the stress concentration effect on fatigue life of CNF/Epoxy. The fatigue stress concentration factor K_f is defined as:

$$K_f = \frac{\text{Fatigue strength without a geometric discontinuity at } N \text{ cycle}}{\text{Fatigue strength with a geometric discontinuity at } N \text{ cycle}}$$

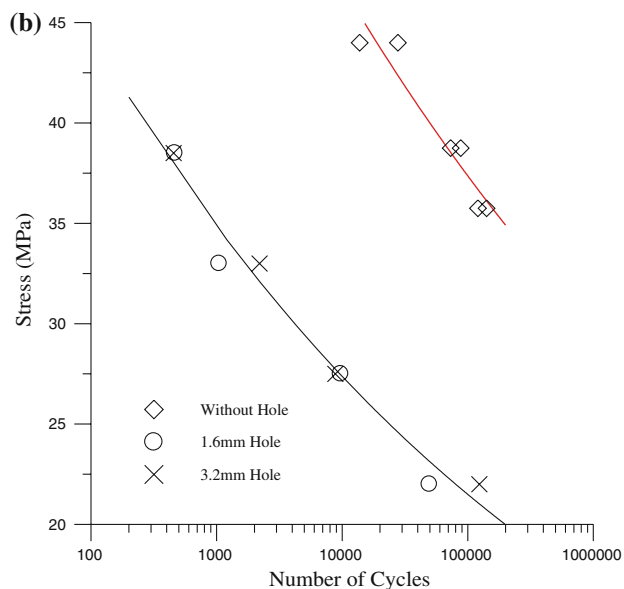
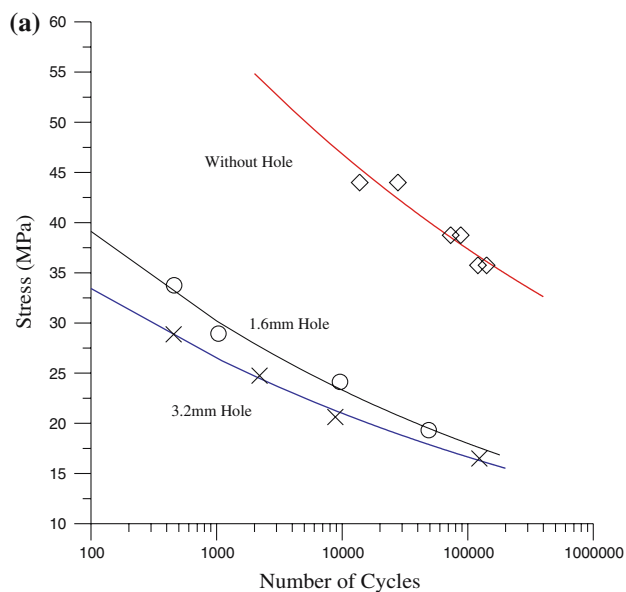


Fig. 11 Effect of stress concentration on fatigue life of 2% CNF/Epoxy

From experimental results, the fatigue stress concentration factor K_f can be simulated as:

$$K_f = 1.60(N_f)^{0.00864}$$

The fatigue stress concentration factor K_f increased with cycle number.

Fracture toughness

Fracture toughness of neat and nanophased epoxy were determined from static tensile of the SENT specimens. Each of these specimens was cycled 100 times between 4% and 40% of the peak load at 1 Hz and then statically tested. During the static tests, the change in specimen length Δl was measured during the tests by recording the ram positions through the displacement transducer of the MTS

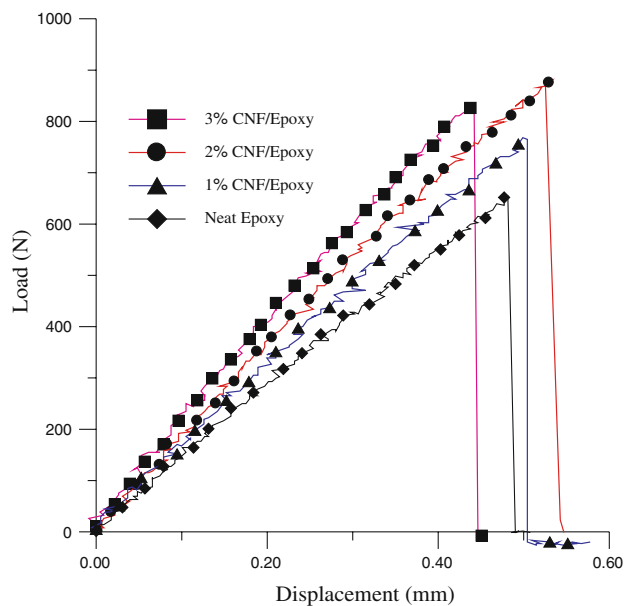


Fig. 12 Load-displacement curves in fracture test

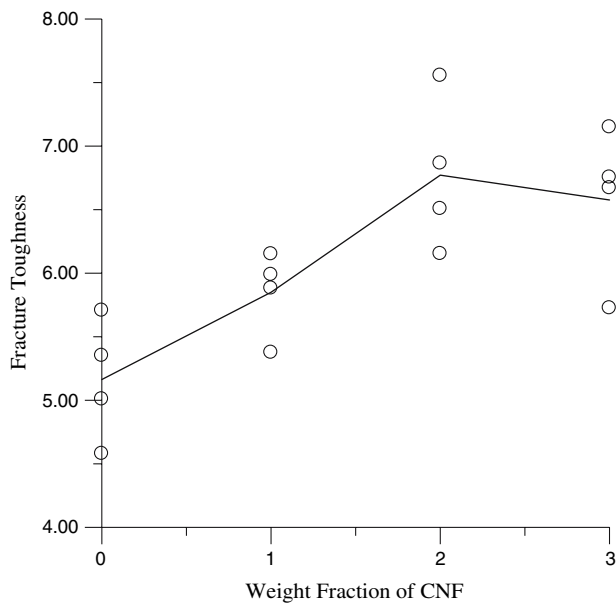


Fig. 13 Effect of CNF contents on fracture toughness

machine. Figure 12 shows the load-displacement diagrams of four materials. Since non-linearity was seldom observed in load-displacement diagrams, the critical stress intensity factor (K_{Ic}) of materials were calculated from peak load of each load-displacement curve, and were plotted as function of CNF weight fraction (as shown in Fig. 13). About 2 wt.% CNF/epoxy exhibited maximum 32% enhancement in fracture toughness. At the higher content, fracture toughness decreased with filler loading.

Fracture surface

To investigate the failure mechanism of neat epoxy and nanophased epoxy, the fracture surfaces of failed specimens were comparatively examined. Fracture surfaces of the same materials at different strain rates are similar, but

the fracture surfaces of materials with different CNF content are different. The micrograph of neat epoxy in Fig. 14a shows a typical fractography feature of brittle fracture behavior, thus accounting for the low fracture toughness of the unfilled epoxy. Generally, a much rougher fracture surface occurs upon adding CNF into the epoxy (Fig. 14b for 2 wt.% system). The increased surface roughness implies that the path of the crack tip is distorted because of the carbon nanofiber, making crack propagation more difficult.

Figure 15a–d show the fracture surface of neat epoxy at different locations and magnifications. The surface near the initial crack is relatively smooth. Obvious cleavage steps and cleavage planes are shown in the specimen (Fig. 15a). Far from initial crack, the fracture surface becomes rougher (Fig. 15b). The rougher surfaces consist of many small cleavage planes (Fig. 15c). Higher magnifications show that second-phased particles have changed the propagation direction of microcracks (Fig. 15d) and the surface is completely flat and featureless between cleavage steps.

Figure 16a and b show the fracture surface of 2 wt.% CNF/epoxy at different magnifications. Rougher surfaces indicate that crack propagation resistance has been enhanced by CNFs. No cleavage steps and cleavage planes were found. Figure 16c clearly shows that in a 2 wt.% system, nanofibers are well separated and uniformly embedded in the epoxy resin. CNF/epoxy interface debonding was also found, indicating a weak interface (Fig. 16c). Figure 16d shows the pulled-out CNF after the interface debonding.

When the CNF content increased to 3 wt.%, the material failure initiated at a large particle that appeared to be an agglomeration of several carbon nanofibers (Fig. 17a). The crack initiation started from the stress concentration caused by the agglomerated CNFs. Figure 17b shows a micrograph of received carbon nanofibers. Many CNFs had already agglomerated. In the acoustic cavitation processing,

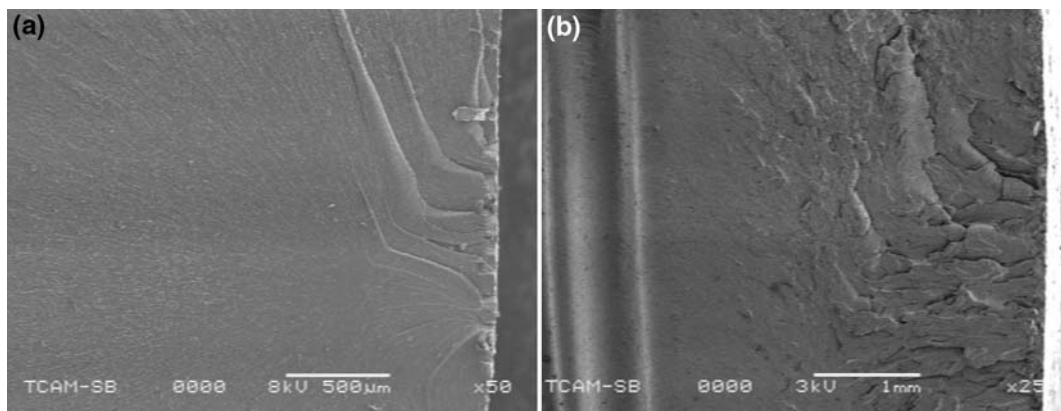


Fig. 14 Fracture surface of neat (a) and nanophased (b) epoxy at low magnification

Fig. 15 Fracture surface of neat epoxy at different location and magnification

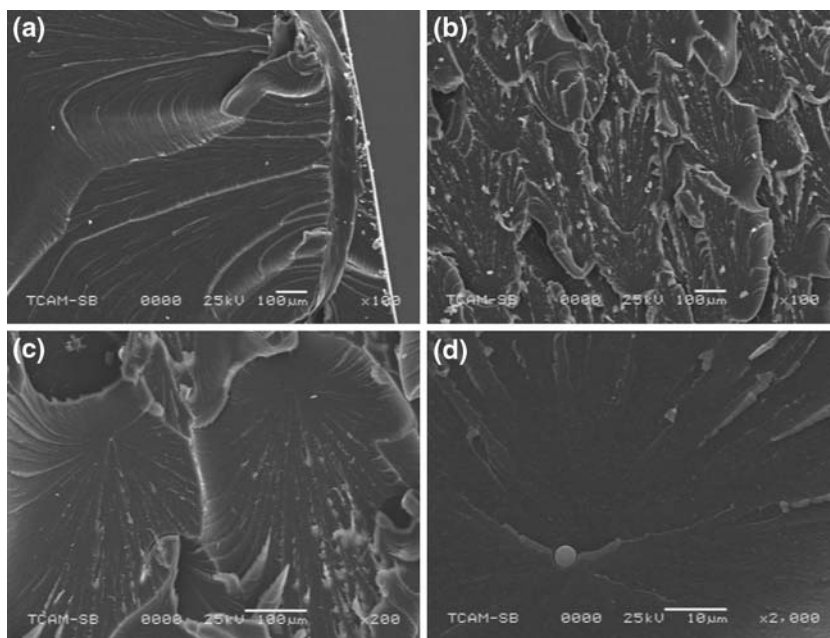
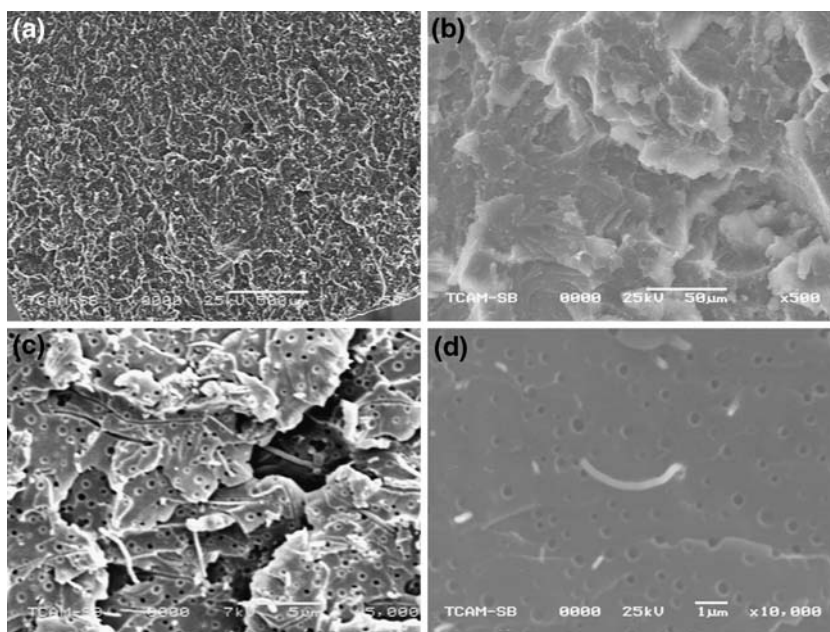


Fig. 16 Fracture surface of 2% CNF/epoxy at different magnification (a: $\times 50$; b: $\times 500$; c: $\times 5,000$ and d: $\times 10,000$)



applying alternating acoustic pressure above the cavitation threshold creates numerous cavities. Agglomerated CNF particles in liquid resin should be broken. But when CNF content is higher than 3 wt.%, ultrasonic mixing can not avoid agglomeration completely.

Conclusion

1. DMA results show that CNF can significantly increase the storage modulus and T_g . TGA results show that the
2. Neat and CNF-modified epoxy are strain rate-dependent materials. The elastic modulus and tensile strength of the materials both increased with higher strain rates, and the relationships between E and $\ln \dot{\epsilon}$ as well as between σ_b and $\ln \dot{\epsilon}$ can be represented by linear function.
3. The tensile, fracture and fatigue results indicate that the 2% CNF infusion system exhibit maximum enhancement as compared with other system.

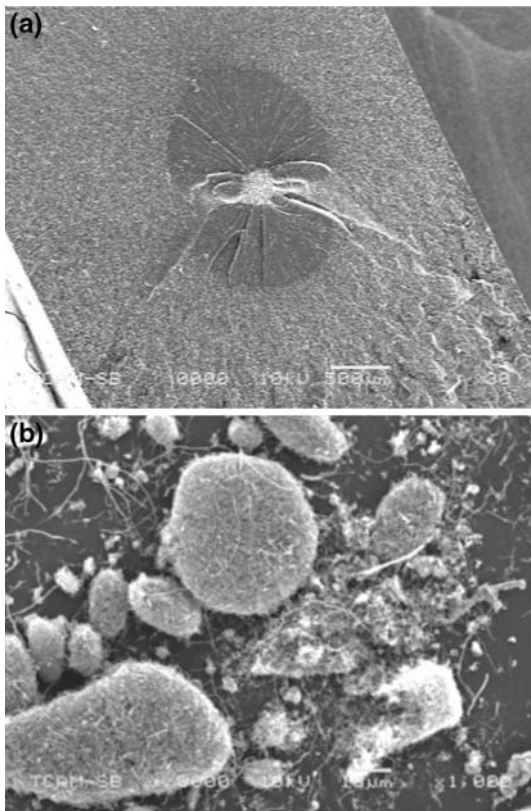


Fig. 17 Fracture surface of 3%CNF/epoxy (a) and agglomerated CNF (b) before the sonication

4. Ultrasonic cavitation is an efficient method of infusing carbon nanotubes into epoxy resin when CNF weight fractions are lower than 2 wt.%. Above the 2 wt.%, CNFs agglomerated.

Acknowledgements The authors would like to gratefully acknowledge the support of National Science Foundation and Department of Energy.

References

1. Donnet JB (2003) *Compos Sci Technol* 63:1085
2. Zheng Y, Zheng Y, Ning R (2003) *Mater Lett* 57:2940
3. Day RJ, Lovell PA, Wazzan AA (2001) *Compos Sci Technol* 61:41
4. Bagheri R, Pearson RA (2001) *Polymer* 41:269
5. Kawaguchi T, Pearson RA (2003) *Polymer* 44:4239
6. Mahfuz H, Adnan A, Rangari VK, Jeelani S, Jang BZ (2004) *Compos: Part A: Appl Sci Manuf*, 35:519
7. Evora VMF, Shukla A (2003) *Mater Sci Eng A* 361:358
8. Hussain M, Oku Y, Nakahira A, Niihara K (1996) *Mater Lett* 26:177
9. Lake ML, Ting JM (1999) Vapor grown carbon fiber composites. In: Burchell TD (ed) *Carbon materials for advanced technologies*. Pergamon Press, Oxford, UK, p 139
10. De Jong KP, Geus JW (2000) *Catal Rev-Sci Eng* 42:481
11. Van Hattum FWJ, Bernardo CA, Finegan JC, Tibbetts GG, Alig RL, Lake ML (1999) *Poly Compos* 20(5):683
12. Gordeyev SA, Macedo FJ, Van Hattum FWJ, Bernardo CA (2000) *Phys B: Condens Matter* 279(1–3):33
13. Tibbetts GG, McHugh JJ (1999) *J Mater Res* 14(7):2871
14. Lozano K, Barrera EV (2000) *J Appl Polym Sci* 79(1):125
15. Lozano K, Bonilla-Rios J, Barrera EV (2001) *J Appl Polym Sci* 80(8):1162
16. Kumar S, Doshi H, Srinivasarao M, Park JO, Schiraldi DA (2002) *Polymer* 43(5):1701
17. Dasch CJ, Baxter WJ, Tibbetts GG (1993) Thermoplastic composites using nanometer-size vapor-grown carbon fibers. 21st Bienn Conf On Carbon. Buffalo, NY, p 82
18. Carneiro OS, Covas JA, Bernardo CA, Caldiera G, Van Hattum FWJ, Ting JM et al (1998) *Compos Sci Technol* 58(3–4):401
19. Caldeira G, Maia JM, Carneiro OS, Covas JA, Bernardo CA, (1998) *Poly Compos* 19(2):147
20. Carneiro OS, Maia JM (2000) *Poly Compos* 21(6):960
21. Carneiro OS, Maia JM (2000) *Poly Compos* 21(6):970
22. Pogue RT, Ye J, Klosterman DA, Glass AS, Chartoff RP (1998) *Compos Part A* 29A(9–10):1273
23. Patton RD, Pittman CU Jr, Wang L, Hill JR (1999) *Compos Part A: Appl Sci Manuf* 30A(9):1081
24. Chellappa V, Chiou ZW, Jang BZ (1994) Electrical behavior of carbon whisker reinforced elastomer matrix composites. Proc 26th SAMPE Tech Conf, p 12